Trabalho de Conclusão de Curso

Resonances in Electron Scattering by Multielectronic Systems: General Aspects of the Theory and Possible Applications

Yan Alexssander Celima de Avó

Centro de Ciências Naturais e Humanas,
Universidade Federal do ABC, Santo André-SP, Brasil

Abstract

In this undergraduate thesis, the focus was on the study of resonances that occur in the scattering of low energy electrons by an atomic or molecular target. A brief historical review, starting from the discovery of the first resonance and the advances achieved in the field since then, will be provided with the intent of putting this subject into an adequate context. The classification for the different types of resonances and the relation between resonances and cross sections will also be discussed. We present an introduction to theoretical methods and experimental techniques employed for determination of the cross sections. The physical interpretation of the resonances is performed through the analysis of case studies involving the atomic hydrogen (H) and helium (He) and the diatomic hydrogen (H$_2$) and tetrahydrofuran (C$_4$H$_8$O) molecules. The importance of resonances' assignment is illustrated in terms of its relevance in applications involving DNA damage and biofuel production. We end by discussing some of the limitations of the theoretical and experimental methods and challenges to be faced by research groups.

Contents

1 Preliminary Considerations

1.1 Introduction

The study of electron scattering by a target (atom, ion or molecule) has been a subject of interest since early 1960's. Even today, the information that can be obtained from investigations related to scattering processes is essential for advances and developments in different areas of the scientific knowledge, such as nuclear physics involving heavy atoms [1], astrophysics [2], quantum chemistry [3], semiconductor and atmospheric physics [4], to mention just a few.

A collision is a physical process where moving particles are forced to deviate from their initial trajectory due to the interaction with a target. The quantitative measure of the result produced by the collision is given by a physical quantity called cross section, i.e., the effective area provided by the target to the incoming projectile and that, in quantum mechanics, specifies the probability with which a given collision process will occur. When dealing with atoms or molecules and depending on the energy of the incident particle, this interaction may lead to changes in the target's internal degrees of freedom. The basic processes which occur in electron-molecule collisions include:

1. $e^-(E_0) + AB \rightarrow e^-(E_0) + AB$ (Elastic scattering)

2. $e^-(E_0) + AB \rightarrow e^-(E) + AB^*$ (Electronic excitation)

3. $e^-(E_0) + AB_{v,j} \rightarrow e^-(E) + AB_{v',j'}$ (Rotational/Vibrational excitation)

4. $e^-(E_0) + AB \rightarrow e^-(E) + A + B$ (Neutral dissociation)

5. $e^-(E_0) + AB \rightarrow 2e^- + AB^+$ (Ionization)

6. $e^-(E_0) + AB \rightarrow 2e^- + A + B^+$ (Dissociative ionization)

7. $e^-(E_0) + AB \rightarrow AB^-$ (Electron attachment)

8. $e^-(E_0) + AB \rightarrow A^- + B$ (Dissociative electron attachment)

where (v,j) and (v',j') represent the vibrational and rotational states of the target before and after the interaction with the incoming electron, respectively.

The focus of this work, as will be discussed below, is on the study of electron collisions by atoms and molecules, with emphasis on analysing the formation of resonant states. In the low energy regime (tipically below 10 eV) electrons can be trapped by the target leading to the formation of a transient state known as "resonance". While describing the process of electron attachment by a target, it is common to use the terms "resonance", "compound state" and "temporary negative ion" interchangeably. The formation of the compound state gives rise to a rapid and pronounced increase on the magnitude of the cross section describing electron collisions by atoms or molecules, as can be seen in Figure 1. In order to provide an adequate assignment for the resonant states it is important to determine their basic characteristics, which are defined in terms of two parameters, namely, the lifetime (τ) and the width (Γ) of the resonance.
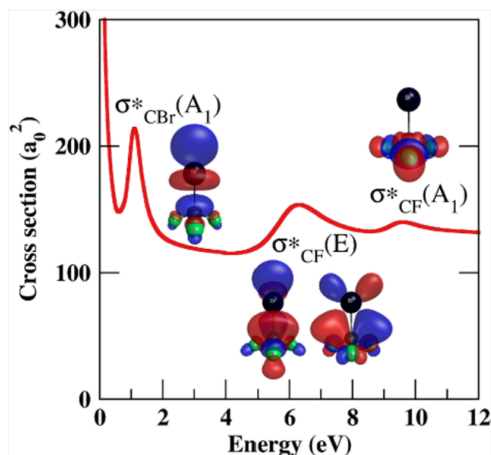
Figure 1: Integral cross section for elastic electron scattering from trifluoroiodomethane (CF_3I) and trifluorobromomethane (CF_3Br) molecules [5]. The resonances can be seen as sharp peaks (as the one around 1 eV) or broader structures (like those centered at 6 eV and 9.5 eV) in the cross sections.

The study of resonances has several applications, ranging from development of new drugs targeted to DNA for cancer treatment in the medical field to the research of reactions taking place in the upper atmosphere. The former implies in a deeper insight into the damage caused to DNA by electron attachment in one of its building blocks and, as a consequence, the development of more efficient radiotherapy procedures. The latter involves the formation of the ionosphere on Earth and other planets, due to the ionization produced by solar ultraviolet (UV) radiation and X-rays. In this case, some photoelectrons produced in the initial step can be energetic enough to cause further ionization, leading to the phenomena named as aurora borealis in the the northern hemisphere or aurora australis in the southern hemisphere [4]. The formation of resonances and assignment of their characteristics have a particular significance during collisions of low energy electrons (LEE) with molecules since LEE species are abundant and the target can undergo chemical modifications via dissociative electron attachment.

Further discussion involving electron collisions by atoms and molecules and the formation of resonances conducted in this work will be limited to the regime of low impact energies and for circumstances in which the radioactive decay (autoionizing state decaying as a product of a photon and the target in the ground or an excited state) can be ignored [6].

1.2 Historical Perspective

First indications of the existence of resonant states can be traced to the paper by J. Franck *et al.* in 1921. At that time, Franck suggested that when an outer-shell electron of the neon atom is promoted to an empty orbital, a second electron can be trapped in this orbital giving rise to an excited negative neon ion [7].

More expressive advances on this subject were only made four decades later, in early 1960's. From the experimental point of view the gap in time can be explained by the difficulty in producing high resolution and intense monoenergetic electron beams. Theoretically, the intrinsic complexity of the quantum mechanical

phenomena involved on the description of electron scattering by multielectronic systems requires the use of approximation methods. The use of approximation methods capable of dealing with this problem only became feasible with the advent of high-speed computers, not available until the beginning of the 1980's.

Renewed interest on the study of resonances took place both theoretically and experimentally in the 1960's with the works of Ugo Fano and George Schulz. In one of his papers, Fano showed that interference of a discrete quasi-stationary state with the adjacent continuum gives rise to resonances in the cross section for elastic and electronically inelastic scattering of electrons by the target [8]. With respect to the work performed by Schulz, we will omit details of his contributions during the 1950's, but in-depth information can be found in the paper "Resonances in atoms and molecules" by Biondi *et al.* [7]. In 1961, Schulz used an electrostatic electron monochromator, aiming to examine the enhanced vibrational excitation for nitrogen between 1.5 and 3.0 eV. The data he obtained provided confirmation that vibrational excitation proceeds very efficiently via a compound state located around 2.3 eV in N_2, that is, the compound state associated with this enhancement was shown to have a vibrational structure [7]. It was only on 1963, while working at the Westinghouse Research Laboratories in Pittsburgh, that Schulz discovered the resonance in the cross section for elastic electron by the helium atom [9]. He also observed a sharp peak in the cross section of neon. Schulz would later publish his findings in the Physical Review Letters, with one of the preprints being sent to Fano, who interpreted the helium resonance as a $(1s2s^2)^2S$ negative ion-state and the neon resonances as a split pair of $(2p^53s^2)^2P_{3/2}$ and $(2p^53s^2)^2P_{1/2}$.
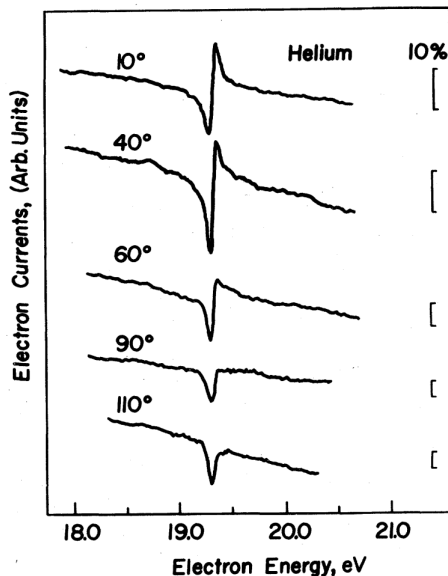
Figure 2: Assignment of the $(1s2s^2)^2S$ resonance in elastic electron scattering by helium for different observation angles, with the vertical lines corresponding to a variation of 10% in the differential cross section [10].

Few years after the discovery of the resonance in the helium atom and its assignment (Figure 2), other resonances were found in helium at higher energies, in other noble gases like argon and xenon atoms [11] and in molecules [12]. By the time of his death in 1976, Schulz was able to examine a large amount of resonances

4

appearing in the cross sections for electron scattering by atoms and molecules and based on these findings he wrote two reviews on the subject [10, 13]. Since then, efforts from experimental and theoretical groups have been devoted to obtain accurate cross sections and to detect the presence of resonances in the different processes that can occur during the electron scattering by atoms and molecules.

2 Theoretical Background

A theoretical explanation of resonances and their parameters can be constructed on the basis of forces of interaction between particles that are treated as elementary particles in such processes.

2.1 Types of Resonance - Classification of Composite States

Before explicitly classifying the resonances, we first introduce the genealogy of resonances. We consider the grandparent as a positive ion. The parent is formed by the interaction of a single electron with the positive ion, resulting in a neutral state. Adding an extra electron to the neutral state will form the "resonance". If the parent lies on the ground state, we have "single-particle resonances", otherwise we will "core-excited resonances" and higher orders ("Doubly core-excited", among others).

There are two distinct types of resonances: "Feshbach resonances" ("Type I resonances" or "closed-channel resonances") and "shape resonances" ("Type II resonances" or "open-channel resonances"). Feshbach resonances are associated with excited parent states and with compound states energetically below the parent state. They arise when the interaction potential between the incident electron and the target in an excited state has enough energy to support the bound state. Type I resonances can decay into the parent state, often presenting a sharp peak near the threshold in the excitation function. The decay into the parent state can be energetically forbidden and, in this case, the compound state decays into a "nonparent" state, resulting in a change in the configuration of the target. The decay into a nonparent state usually indicates a narrow width and higher lifetime.

Shape resonances are associated with ground and excited parent states and with compound states energetically above the parent state. They arise when the potential forms a barrier which captures the incident electron within the target in a resonance orbital. The transient state normally decays into the parent state, indicating a larger width and shorter lifetime when compared to Feshbach resonances. This type of resonance appears only when the incident electron possesses an angular momentum relative to the target, i.e., electron s-wave resonances ($l = 0$) do not produce a barrier. A summary of the different resonances, along with examples and some characteristics can be seen in Figure 3.

The autoionizing states formed during the capture of the incident electron would decay in a time $\tau \sim 1/\Gamma$ (Breit-Wigner distribution) into the target and an electron in the continuum spectrum. The most probable autoionizing state decay is the next-lowest state of the multielectronic system on the energy scale, provided that conservation laws do not prevent this decay. The processes energetically allowed determine the open channels. The energetically prohibited processes determine the closed channels. After the electron emission,

First name	Last name	Parent	Energy *vis a vis* parent	Some characteristics	Examples
Single-particle Shape (1 particle, 0 holes)	⋯	Ground electronic state	above (0–4 eV)	Vibrational excitation; dissociative attachment at low energy	N₂ (2.3 eV) H₂ (2–4 eV)
Core-excited Particle–hole (2 particles, 1 hole)	Feshbach; Type I; closed-channel	Mostly Rydberg excited state	below (∼0.5 eV)	Bands correlated to grandparent; sharp structure; many decay channels	N₂ (11.48 eV) H₂ (Bands "a"– "g")
	Shape; Type II; open-channel	Rydberg or valence excited state	above (0–2 eV)	Dissociative attachment	N₂ (9–11 eV) H₂ (8–12 eV)
Doubly core-excited (3 particles, 2 holes)	Feshbach	Doubly excited Rydberg and valence states	below	Above ionization; 2-electron decay	He (57.16 eV)
	Shape		above		N₂ (22 eV)

Figure 3: Semantics of resonances. Information regarding the parent state prior to the electron interaction and energetic relation of the compound state with parent target is presented. Characteristics of different resonances are also showed [13].

the target may decay into different final states. Each final state is called as a "channel", so we use "channels of decay" for a particular resonance. For a given resonance, the branching ratio favors a particular decay, making easier to detect the most probable final state by experimentally measuring the scattering cross section-versus-energy curves. Some channels of decay can induce bond breaks in the target via dissociative electron attachment (DEA).

At sufficiently low impact energies (up to 1% energy difference between the relativistic and non-relativistic energies), the relativistic effects can be neglected and the description of the scattering problem can be obtained by solving the Schrödinger's equation:

$$(H - E)\Psi = 0 \tag{1}$$

It is important to note that apart from the harmonic oscillator and hydrogen-like atoms almost all other quantum systems cannot be solved exactly, requiring the use of approximation methods to be handled.

As indicated on top of Figure 4, the incident electron with energy E_0 and represented by a plane wave with wavenumber $\overrightarrow{k_i}$ is scattered in the direction of the vector $\overrightarrow{k_f}$ at an angle θ with respect to the direction of the incident particle. The scattered electron is described by an emergent spherical wave modulated by the scattering amplitude $f(\Omega)$, where $\Omega = (\theta, \phi)$. Thus, considering that the electron-molecule interaction is described by a potential $V(\overrightarrow{r})$, the asymptotic scattering or diffraction pattern is described by the wave function:

$$\Psi_{r\to\infty} \to e^{i\overrightarrow{k_i}\cdot\overrightarrow{r}} + f(\Omega)\frac{e^{ik_f r}}{r} \tag{2}$$

where the first and second terms in the right-hand side in the above equation represent the incoming plane wave and the emerging spherical wave, respectively. Differential cross section (DCS) for a scattering process is given by:

$$\frac{d\sigma}{d\Omega} = \frac{k_f}{k_i} |f(\Omega)|^2 \tag{3}$$

The integral cross section (ICS) for a given scattering process is obtained by integration of the corresponding DCSs over all scattering angles

$$\sigma_i = 2\pi \int_0^\pi \frac{d\sigma}{d\Omega} sin\theta d\theta \tag{4}$$

and the total cross section (TCS) is given by the sum of the ICSs for all scattering events energetically allowed to the electron-target system during the collision:

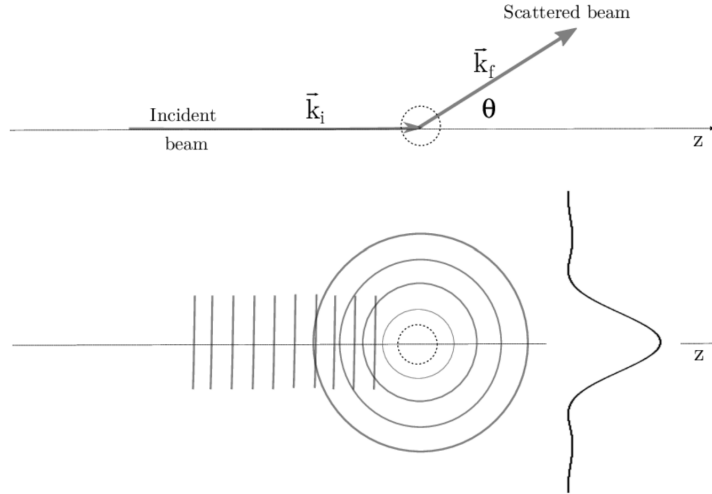$$\sigma_T = \sum_n \sigma_n(E) \tag{5}$$

Figure 4: General representation for an electron-target scattering process. In the bottom of the figure the incident electron is represented by a plane wave while the scattered electron is represented by an emerging spherical wave [14].

7

2.2 Approximation Methods

2.2.1 Schwinger multichannel method

The Schwinger multichannel (SMC) method is an *ab initio* method developed by Takatsuka and McKoy [15, 16] and obtained as an extension of the Schwinger variational principle (SVP). The SVP is used for nonidentical collisions, but not for identical particle collisions. Details regarding formulation have been given elsewhere [15]. The first version of the SMC method relied on a Cartesian Gaussian projector insertion technique. As a result, this version needed a large number of trials of Cartesian Gaussian functions and was not precise. After a number of steps to optimize the method, two different versions of the program were evolved upon. The version at Caltech [17], and the version at State University of Campinas (UNICAMP), which implemented norm-conserving pseudopotentials into the method (SMCPP) [18].

The SMC is a variational method that uses $(N+1)$-particle square-integrable basis (L^2) wave functions to obtain the scattering amplitude for the collision. Its implementations considers the fixed-nuclei approximation and includes effects such as polarization, exchange and electronic multichannel coupling. The SMC method incorporates both open- and closed-channel spaces into electron-target collisions via a projected Lippmann-Schwinger and Schrödinger equations, respectively. For this variational method they expand the scattering wave function in a trial basis set,

$$\left| \Psi_{\vec{k}}^{(\pm)} \right\rangle = \sum_m a_m^{(\pm)}(\vec{k}) \left| \chi_m \right\rangle; \tag{6}$$

the coefficients $a_m^{(\pm)}(\vec{k})$ allows us to write the expression for the scattering amplitude as

$$f_B^{SMC}(\vec{k_f}, \vec{k_i}) = -\frac{1}{2\pi} \sum_{m,n} \left\langle S_{\vec{k_i}} \left| V \right| \chi_m \right\rangle (d^{-1})_{mn} \left\langle \chi_n \left| V \right| S_{\vec{k_f}} \right\rangle, \tag{7}$$

where the $\{ |\chi_m\rangle \}$ represents a basis set of $(N+1)$-electron symmetry-adapted Slater determinants and V is the interaction potential. Also, $S_{\vec{k}_{i,f}}$ are products of a target wave function and a plane wave and where

$$d_{mn} = \left\langle \chi_m \left| A^{(+)} \right| \chi_n \right\rangle \tag{8}$$

The implementation of SMC method for the work of da Costa *et al.* [19] rewrote the formula for the operator $A^{(+)}$ in the following way:

$$A^{(+)} = \left[PV - VG_P^{(+)}V + \hat{H}\left(\frac{1}{N+1} - P \right) \right] \tag{9}$$

The matrix elements of $A^{(+)}$, when symmetrized, are equivalent the matrix elements obtained by usual means [20]. In equation 9, P is a projector operator onto the open-channel space spanned by the target eigenfunctions, $G_P^{(+)}$ is Green's function projected on the P-space and $\hat{H}$ is the total Hamiltonian. Equation 7 provides an analytical approximation to the scattering amplitude in the body reference frame. To obtain cross sections that can be compared by experimental measurements, $f_B^{SMC}(\overrightarrow{k}_f, \overrightarrow{k}_i)$ can be expanded in partial waves [21].

For a target, the description of the many-body dynamics in the collision is affected by the inclusion and the balanced treatment of the proper effects (polarization, exchange, multichannel coupling effects). When impact energies are sufficiently low, only the elastic channel opens (energetically accessible) and the collision process is dominated by the description of how the incident electron distorts the electronic cloud of the target, an effect which is taken into account by allowing virtual excitations (closed channel space) from the ground state. The Static-Exchange plus Polarization (SEP) approximation level combines the virtual excitation effect with the correct solution of the scattering problem. With increasing electron impact energy, several discrete and continuum states (above the ionization threshold) become energetically accessible, giving rise to the multichannel coupling effect.

The possibility of multiple channels leads to competition effects among the possible states at a given energy, which results in some statistically favoured channels. Each accessible state would have to be included in the scattering calculation to properly obtain the flux distribution among participant channels. As the incident electron energy increases, a larger number of electronic states become energetically accessible, therefore, the inclusion of all channels for complex molecules and for higher incident electron energy calculations demands high computational costs. The high demand can be somewhat mitigated by evaluating the cost-effectiveness of different functions (polarization, diffusion) and by selecting the more favourable channels for the calculations. In scattering calculation each new threshold (channel opened) affects the cross section, so upcoming channel can give rise to resonances on the target.

2.2.2   R-matrix method

Initially, *ab initio* calculation of the R-matrix was not possible, since the physics of the system enclosed within the sphere were not known, i.e., no solution was obtained for the inner region. Instead, the method is parameterized on the boundary, and only the energy dependence of the outer region was studied [22]. The first *ab initio* R-matrix methods were developed for atoms [23], later being developed for molecules [24]. In larger molecules, where an accurate *ab initio* solution is not yet possible, the R-matrix is still used to parameterize resonances [25].

The R-matrix method is based on the division of the configuration space into inner and outer regions. The boundary between the regions is a parameter known as the channel radius. Choosing the radius a of the R-matrix sphere is critical since the charge densities of the relevant N-electron target states and the $(N + 1)$-electron configurations must be contained inside the inner region for the method to be valid (Figure 5) [26]. The inner region uses a set of basis functions to describe the system of $(N + 1)$-electron by taking several aspects into consideration: spin and space coordinates, square-integrable basis, diagonalisation of the

Hamiltonian, among others. In the outer region, the interaction between the scattering electron and the target molecule is approximated by a single-center multiple potential expansion.

The R-matrix allows parametrization of various physical processes and its determination provides collision matrices and cross sections. A well chosen square-integrable basis can provide accurate approximations of scattering wave functions over the internal region. The choice of target electronic states to be included in the scattering calculations and the type of L^2 functions used to describe these states defines the scattering model. This choice is restricted by the standard R-matrix requirement of keeping the wave function within the R-matrix sphere; this tends to rule out the use of very extended basis sets which usually contain a considerable number of diffuse functions.

In the fixed nuclei approximation, the Schrödinger equation for an $(N + 1)$ electron target system is:

$$(\hat{H} - E_k) \left| \Psi_k^{N+1} \right\rangle = 0 \tag{10}$$

To consider the finite volume of the sphere, an extra term needs to be included to keep the Hamiltonian Hermitian, the Bloch operator $\hat{\mathbf{L}}_b$:

$$(\hat{H} + \hat{\mathbf{L}}_b - E_k) \left| \Psi_k^{N+1} \right\rangle = \hat{\mathbf{L}}_b \left| \Psi_k^{N+1} \right\rangle \tag{11}$$

The eigenfunctions of the Hamiltonian form a complete basis set inside this region. A solution to the Schrödinger equation, eq. 11, can be written in terms of these functions;

$$\Psi^{N+1} = \sum_k A_k(E) \Psi_k^{N+1} \tag{12}$$

The inner region basis functions are constructed using the close-coupling (CC) approximation, and take the form:

$$\Psi_k^{N+1} = \hat{A} \sum_{ij} a_{ijk} \Phi_i^N(\mathbf{x}_1 \cdots \mathbf{x}_N) u_{ij}(\mathbf{x}_{N+1}) + \sum_i b_{ik} \chi_i^{N+1}(\mathbf{x}_1 \cdots \mathbf{x}_{N+1}) \tag{13}$$

where Φ_i^N is the wavefunction of the ith target state and is itself represented by a sum over target configurations,

$$\Phi_i^N = \sum_m c_{im} \chi_m^N(\mathbf{x}_1 \cdots \mathbf{x}_N) \tag{14}$$

10

In the CC approximation, a number of target electronic excited states are included, normally described at the complete active space (CAS) level. The active space includes both occupied and unoccupied orbitals of the ground state configuration. In eq. 13, a_{ijk} is the coefficient of the ith target times the jth continuum orbital in the kth inner region wave function, b_{ik} the ith L^2 configuration in the kth inner region wave function, χ_i^{N+1} is the ith $(N+1)$ electron L^2 Configuration State Function (CSF). The electrons in the scattering wavefunction must obey the Pauli principle, and are therefore anti-symmetrized by the operator $\hat{A}$. In eq. 14, the c_{im} is the coefficient of the mth CSF in the ith target wavefunction. Further discussion regarding the wavefunction for the R-matrix method is found elsewhere [27].

In the outer region, the interaction between the scattering electron and the target molecule is approximated by a single-centre multiple potential expansion. The basis functions Ψ_k^{N+1} are used to construct the R-matrix at the boundary between the regions. This R-matrix is propagated to the asymptotic region, where by matching with known asymptotic expressions, the K-matrix is determined. From the K-matrix one can extract resonance parameters (energy and width) as well as determine cross sections via the T-matrix [28].

Other level of approximation used with the R-matrix method is the static-exchange plus polarization (SEP). At the SEP level, only the target ground state wavefunction is included. The multielectronic system can be polarized by the incoming electron; this effect is described by inclusion of appropriate L^2 configurations. The SEP models are suited to shape resonances for the target initially in the ground state. The method can also describe, poorly, core-excited resonances associated with single excitations of the target molecule. In the SEP model, the target molecule is described at the Hartree-Fock level.
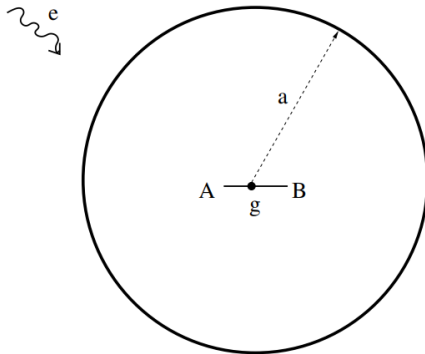

Figure 5: Visual representation of R-matrix method division of space into inner and outer regions. The boundary is a sphere of radius a centered on the center-of-mass of the target (g). The outer region contains a single incident electron. The inner region contains the wave function of the target (A and B) [26].

When dealing with highly extended target wave functions, such as those found in Rydberg states, or when dealing with geometrically large molecules, R-matrix method can lead to problems. In contrast, inner region problems are solved independently of the scattering electron's energy, with the dependence on the energy only affecting solutions in the outer region. Therefore R-matrix method is of particular interest for studying resonances and determining resonance parameters.

3   Experimental Techniques

As mentioned before, resonances manifest themselves as pronounced structures in the cross section curves describing the electron scattering by atoms and molecules. Therefore, the experimental determination of the resonant structures implies in obtaining the different types of cross sections that represent collision processes driven by electron impact.

Before Schulz's discovery of the helium resonance in 1963, different experimental techniques were developed for the study of collisions in atomic and nuclear physics, but the lack of intense and highly collimated beams at that time restricted the application of these techniques to detection of resonances since, in general, they occur in a very narrow range of energies.

In the first paper regarding resonances published by Schulz, he used a double electrostatic analyzer as depicted in Figure 6. For this arrangement, the first electrostatic analyzer was used for the production of an electron beam with a half-width of 0.06 eV. The electrons are accelerated into the collision chamber where they are crossed with a beam of helium atoms. Electrons elastically scattered at an angle of 72° are admitted to the second electrostatic analyzer and passed through a slit into an electron multiplier. A vibrating reed electrometer is then used to measure the electric current. By using this apparatus, a resonance was found for electrons scattered at 72° with an energy of approximately 19.3 eV, below the onset of the helium's first excited state (19.8 eV), as already shown in Figure 2 [9].
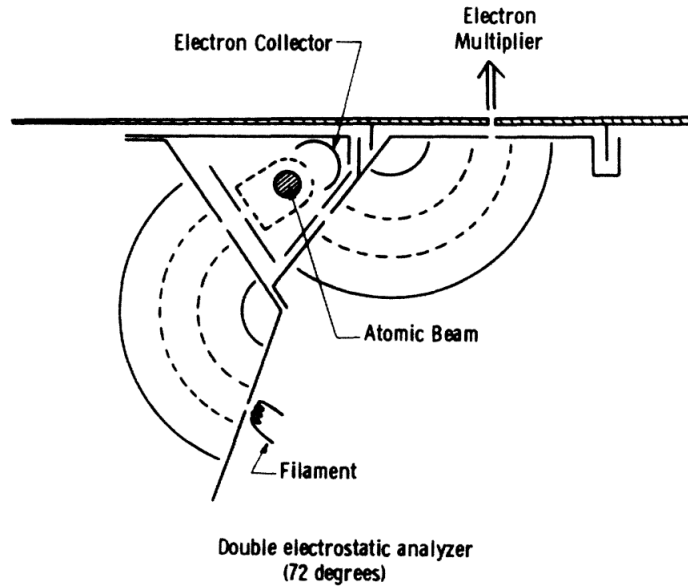

Figure 6: Schematic representation of the double electrostatic analyzer used by Schulz in the investigations that lead to the discovery of the $(1s2s^2)^2$S resonance in helium [9].

While the electron monochromator and the collision chamber remains as basic components in virtually all experimental arrangements built thenceforth, detection techniques would differ considerably from each other depending on the type of cross section to be measured, as can be seen in Figure 7.
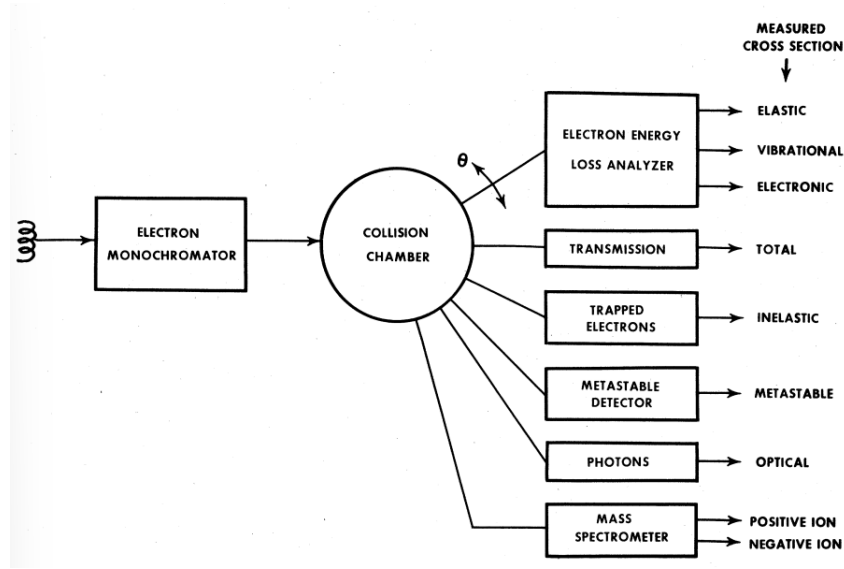
Figure 7: Pictorial scheme of the relationship between the experimental techniques and the different types of cross sections that can be measured. [10].

In the following, we will present a brief discussion of some techniques used to obtain the differential and integral cross sections for elastic scattering, rotational, vibrational and electronic excitation, as well as the total cross section. An extensive review and more details on the experimental techniques presented here can be found elsewhere [29, 10].

3.1   Total scattering cross section measurements

According to the definition presented in section 2, the TCS is given by the sum of the ICSs for all collision processes accessible to the target at a given electron impact energy (see Eq. 5). Due to the intrinsic character inherent to its nature, the TCS provides a measure for the probability of occurrence of the electron-target collision, but without an indication about the specific type of scattering process (elastic, inelastic, etc.) involved in the electron-target interaction.

The most commonly used technique for determining TCSs is the "transmission method". In this method the cross sections are obtained by measuring the attenuation of the electron beam passing through the target gas. As schematically represented in Figure 8, electrons pass through the gas until each undergoes a collision at random and is removed from the initial beam. Thus, the intensity of the beam will continuously drop and the mean kinetic energy of the electrons will also generally decrease. The degradation of the beam intensity follows the Beer-Lambert exponential attenuation law [30] and all that is required, in principle, is the ratio of the initial (I_0) and transmitted electron beam intensities (I_t) as a function of the target pressure. When working with this technique, problems regarding multiple scattering and space charge effects may arise. Since a considerable fraction of the scattering is related to inelastic processes, these problems can be mitigated by using a retarding potential analyzer [31].
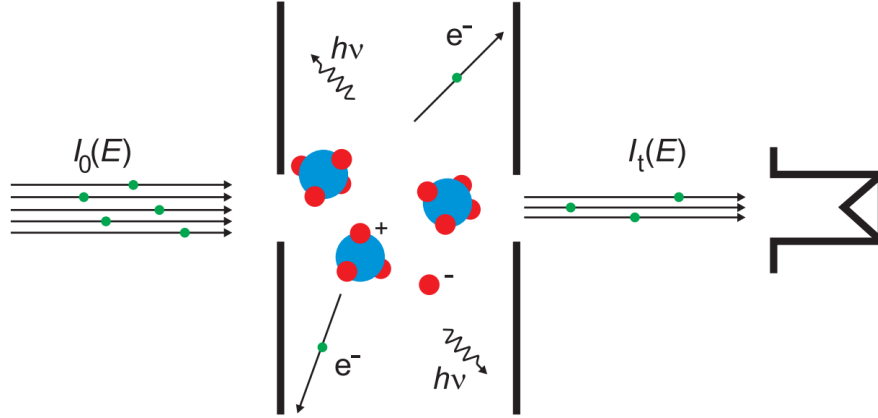
Figure 8: Pictorial representation of the electron transmission method [32], where I_0 and I_t are the initial and transmitted electron beam intensities, respectively.

The "recoil" and "time-of-flight" techniques, build upon the transmission technique, can also be used for TCS measurements. In contrast to the transmission method, in the recoil technique it is the molecular beam rather than the electron beam that is measured. The drawback in this case is related to the need of a high angular resolution and an accurate detection of neutral molecules [33]. In the time-of-flight method the temporal distribution of the electron beam signal is converted to an energy distribution with the use of an empty gas cell. When an amount of gas is introduced in the cell, the attenuation of the electron beam as a function of energy (time distribution) can be determined and related to the total scattering cross section as it is done in other types of transmission experiments. The time-of-flight approach avoids some of the problems common to conventional transmission methods, however, the experimental setup it is limited to operate at low impact energies (below few tenths of an electron-volt) by flux and at high impact energies (above 50 eV) by time resolution.

3.2   Differential cross section measurements

The measurement of DCSs is, at least in principle, straightforward. All that is needed is to cross the electron and gas target beams and then to analyse the scattered electrons arriving at a detector of infinite angular resolution (Figure 9) located at a sufficiently large distance from the interaction region. For a specific impact energy, the DCS is given as a function of the scattering angle (θ).

The use of crossed beam methods is of particular relevance for determining the DCSs because in this kind of experiment the cross section averaged over the instrumental angular and energetic resolution is proportional to the intensity of the scattered beam (Figure 10). In fact, this was the technique employed by Schulz in the double electrostatic analyzer experiment previously described. The measurement of DCSs is, in most of the experimental devices currently available, typically limited to the angular range $20° \leq \theta_{measured} \leq 150°$, and these limit values strongly depend on the electron beam energy of study, the technique employed and
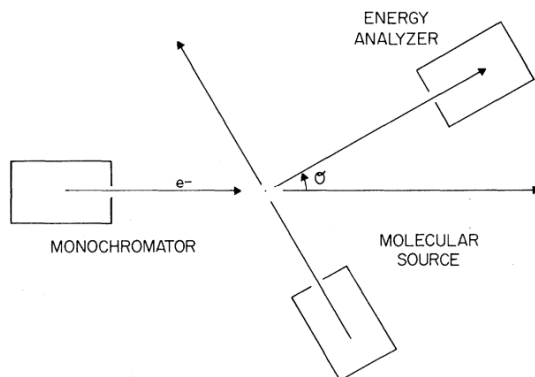
Figure 9: Pictorial representation of the experimental setup for measurement of differential scattering cross sections [34].

whether the collision is elastic or inelastic [35, 36]. The upper limit on the angular range is set by the physical dimensions of the energy selector and analyser. For small angles, the correction for the effective path length changes very drastically for processes with a strongly forward-peaked DCS. This is due to the fact that an instrument with a finite angular resolution integrates the signal over a range of angles (positive and negative) over which the cross section changes very rapidly. Another reason is that the direct beam at zero angle enters the detector and causes background problems. A third reason is that small errors in determining the scattering angle cause large variations in the cross section data [37]. Consequently, techniques to extrapolate the differential cross sections near to 0° and 180° must be employed.
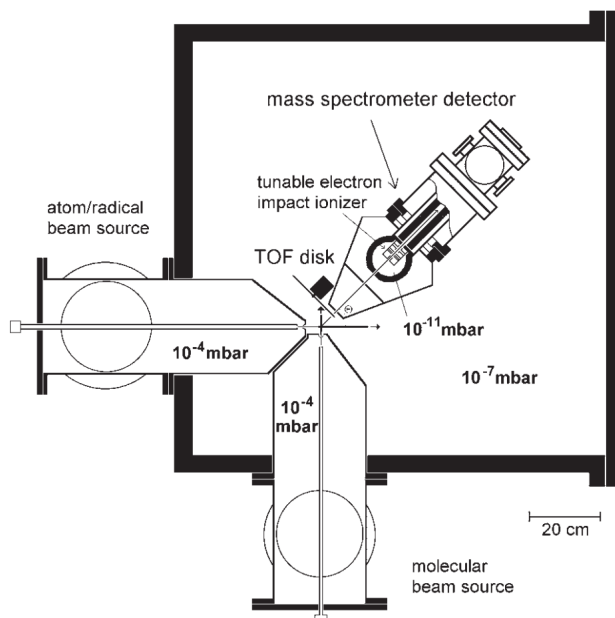

Figure 10: Schematic representation of a crossed molecular beam apparatus [38].

There are several techniques used by the experimental groups to extrapolate the DCS data near to 0°

15

and 180°, but we shall mention only two of them. In the first method, employed for elastic and inelastic scattering, theoretical cross sections were used to guide the extrapolation process. The second technique was outlined by Lun *et al.* [39] and Sun *et al.* [40] and it is based on the inverse scattering theory. A limiting aspect related to this procedure is that, for equipment in which scattered electrons are detected, ICSs are obtained from DCSs by numerical integration over all scattering angles (Eq. 4) and the use of extrapolation methods usually lead to a significant increase in the error bars, especially in the range of low impact energies.

4 Review of Results by Case Studies

4.1 Atomic Hydrogen

From the theoretical viewpoint, the atomic hydrogen is the simplest system for the calculation of resonances. The first indication of resonances in the scattering electrons by atomic hydrogen came from the theoretical work of Burke and Schey in 1962 [41]. In their work, the resonance was identified in the lowest state of the target atom (atomic term ^{1}S), lying about 0.6 eV below the $n = 2$ state of hydrogen.

The first confirmation of the theoretical considerations was obtained in the elastic cross section experiment of Schulz (1964a) [42] who found a peak in the electron current transmitted through atomic hydrogen at an electron energy of 9.70 ± 0.15 eV, however, due to limitations in the resolution, it was not possible to identify whether the resonance was in an ^{1}S or ^{3}P states. In 1972, Sanche and Burrow succeeded in resolving these states in a transmission experiment (Figure 11) [43].
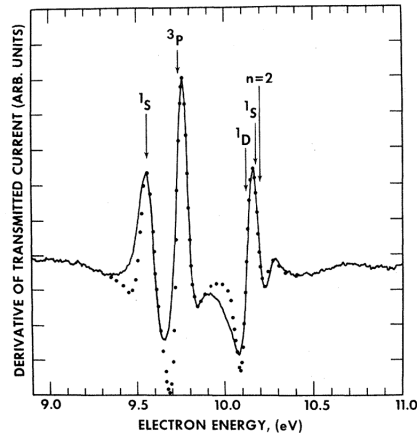

Figure 11: The solid line shows the derivative of the transmitted current through atomic hydrogen measured as a function of the electron impact energy. The arrows indicate the positions of the resonances predicted theoretically, in which atomic state the resonance was found and the threshold for excitation to the $n = 2$ level. The solid circles are the results of an optimum fit to the experimental data from which the resonance parameters were derived [43].

4.2   Helium

Helium is the second most abundant element in the universe and has many academic and industrial applications. For these reasons, obtaining reliable data for processes involving the helium atom is of immense importance, with electron-scattering cross sections providing valuable information. Since helium is one of the simpler complex atoms for which a large amount of experimental data are available, it also provides an ideal testing ground for developing a general method for electron scattering from complex atomic and ionic targets.

In the neighbourhood of the $n = 2$ threshold, there are three resonances that play a major role in the energy dependence of the cross sections. The first resonance was identified in the $(1s2s^2)^2$S state , below the 2^3S ionization threshold. The other two resonances were found in the $(1s2s2p)^2$P and $(1s2s3d)^2$D states, below the 2^1P threshold [44].

Applying the R-matrix with pseudostates (RMPS) method and fitting the eigenphase for the S wave, Hudson *et al.* [45] obtained the position for the ^{2}S resonance as 19.366 eV with a width of 10.7 meV. These result is in good agreement with the experimental results of Cvejanović *et al.* (1974) [46], Brunt *et al.* (1977) [47], and Kennerly *et al.* (1981) [48] who found positions of 19.367±0.009 eV, 19.367±0.007 eV, and 19.37 eV, respectively for the ^{2}S resonance (Figure 12). The width of the resonance was 9 ± 1 meV for Cvejanović *et al.* and 11.0 ± 0.5 meV for Kennerly *et al.*. An extensive discussion on P and D resonances and more results of S resonances presented here can be found elsewhere [45].
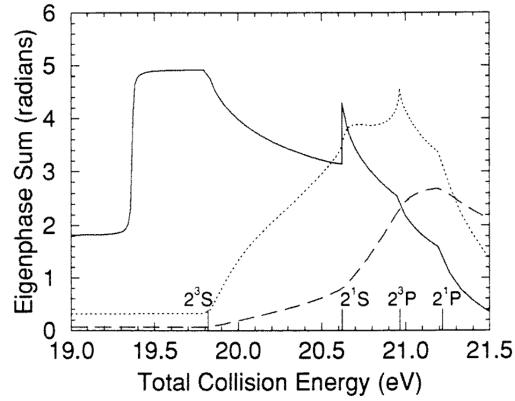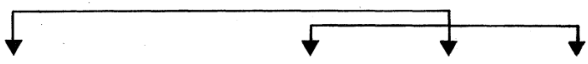

Figure 12: The ^{2}S (full curve), ^{2}P^0 (dotted curve), and ^{2}D (broken curve) eigenphase sums (in radians) near the $n = 2$ thresholds marked by the long tickmarks [45].

4.3   Molecular Hydrogen

The hydrogen molecule H_2 is the simplest molecule in nature. It is the most abundant molecule in universe, particularly in interstellar space. It is also the main constituent in the atmospheres of the outer planets. Plasmas containing H_2 are widely used in plasma technology for applications such as thin film deposition and material treatment. For this reason, among other, H_2 has been a subject of numerous experimental studies [33, 49, 50] and serves as testing ground for theoretical models and approximations.

For H_2 in the ground state, the incident electron can occupy the molecule's lowest unfilled orbital, forming its lowest resonance. Bardsley *et al.* [51] and Eliezer *et al.* [52] found that the ground state of H_2^- is a shape resonance and its designation is $^2\sum_u^+$ [13]. There is little evidence for the $^2\sum_u^+$ state in the elastic cross section due to the short lifetime and large width. Therefore, one has to study other decay channels to establish the existence of this state, such as vibrational and rotational excitations, and dissociative attachment. A summary of experimental data on H_2^- can be seen in Figure 13.

	"a"	"b"	"c"	"d"	"e"	"f"	"g"
Possible equivalence[a]							
Band designation	"a"	"b"	"c"	"d"	"e"	"f"	"g"
Kuyatt *et al.* (1966) (transmission)	"strong" 11.28	$\times$[e]	"weak" 11.46				
Comer and Read (1971a)	$X\,^1\Sigma_g^+(v)$ 11.30	$X\,^1\Sigma_g^+$ $(v>8)$ 10.93[f]	$X\,^1\Sigma_g^+(v)$ 11.19[g]				
Weingartshofer *et al.* (1970)	"Series I" $X\,^1\Sigma_g^+,\,b\,^3\Sigma_u^+$ 11.30			"Series I" $B\,^1\Sigma_u^+$ 11.30	"Series II" $B\,^1\Sigma_u^+$ 11.50	$C\,^1\Pi_u$ 13.63	
Sanche and Schulz (transmission) (1972)	11.32	$\times$	11.43			13.66	15.09
Width, Γ (eV)	≤ 0.016 (H_2)[g] 0.03 (D_2)	0.03[e]	<0.016[g]			0.08[b]	
Symmetry	$^2\Sigma_g^+$	$^2\Sigma_g^+$	$^2\Sigma_g^+$; $^2\Pi_u$	$^2\Pi_g$ (?)		$^2\Sigma_g^+$	
Observed in	H_2, HD, D_2	H_2	H_2, HD, D_2	H_2	H_2	H_2, D_2	H_2, D_2
R_e (Å)[e]	0.97 ± 0.01	1.175 ± 0.01		0.97			
a (eV)[e,d]	0.345 ± 0.015	0.19 ± 0.015		0.345			
b (eV)[e,d]	0.0135 ± 0.003	0.005 ± 0.003		0.0135			
E_0 (eV)[e,d]	11.40	11.11		11.40			

[a] The arrows indicate that band "a" could be identical to band "d" and that band "c" may be identical to band "e." See text.
[b] From Weingartshofer *et al.* (1970).
[e] From Comer and Read (1971a).
[d] Defined by the equation $E = E_0 + a(v+\frac{1}{2}) - b(v+\frac{1}{2})^2$.
[e] The symbol $\times$ indicates that band "b" is observable only in the high vibrational states $(v>8)$ of the $^1\Sigma_g^+$ state and thus cannot be observed in transmission experiments.
[f] Extrapolated to $v=0$; see Appendix I.
[g] From Joyez, Comer, and Read (1973).

Figure 13: For each author, its given the nomenclature they used for a given band, the final state in which the band was observed and the energy of the first resonance, in eV [13].

4.4 Tetrahydrofuran

Since the demonstration by Sanche and coworkers [53] that low energy electrons can induce DNA strand breaks, there has been considerable attention paid to electron collision processes involving constituents of DNA. In particular, low energy electron interactions with tetrahydrofuran (THF: C_4H_8O), the simplest model of the furanose ring that links the phosphate groups in the DNA backbone, have been studied intensively.

18

A summary of different theoretical and experimental techniques applied to LEE scattering by THF can be seen in the work of Gauf *et al.* (2012) [54]. These authors used an electron-impact spectrometer designed for small angle scattering measurements to obtain the DCS data.

Additionally, Gauf *et al.* computed the elastic cross section for electron scattering by THF within the fixed-nuclei approximation using the SMC method as implemented for parallel computers. The molecular structure was taken to be the conformer having C_2 point-group symmetry. Electron scattering by a strongly polar molecule such as THF is heavily influenced by the dipole potential, so the "Born completion" procedure was applied to complement the results obtained from the SMC method.

At most energies and angles, there is an excellent agreement between measured and calculated differential cross sections for energies as low as 1 eV (Figure 14), but only if long-range scattering from the dipole potential is included in the calculation. Both results obtained at fixed angles as a function of energy and angle-integrated results reflect the existence of several shape resonances, which is expected for larger multielectronic systems.
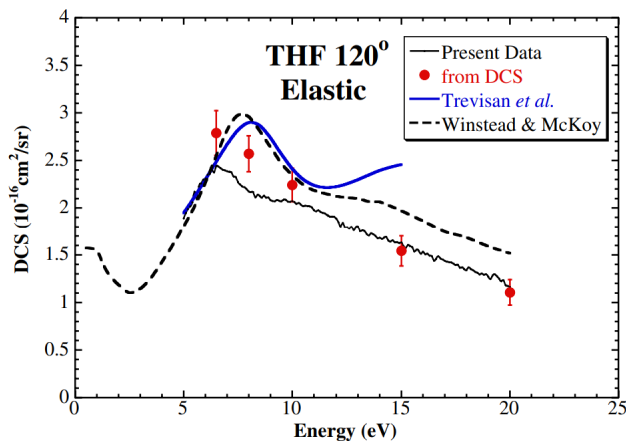
Figure 14: Absolute excitation function for elastic scattering for THF at 120°. A broad shape resonance is observed at around 8 eV for the theoretical calculations, while in the experimental measurement of Colyer *et al.* it is observed at around 6.5 eV [55].

5 Applications

5.1 Biofuel Production

Biofuel production from renewable sources is an alternative to replace fossil fuels, either partially or completely, helping to reduce the emission of greenhouse gases. A major interest of the biofuel industry is the development of efficient methods to obtain fermentable sugars from lignocellulosic biomass, e.g. leaves, straw and bagasse. Biomass is a composite material that mainly consists of cellulose fibres ($\sim 45\%$ content) tightly embedded within hemicellulose ($\sim 30\%$ content) and lignin ($\sim 25\%$ content). The latter is an aromatic copolymer

that confers mechanical strength to lignocellulosic materials, while hemicellulose and cellulose are saturated polysaccharides.

Though the basic units of cellulose are fermentable sugars, the lignocellulose complex structure makes the biomass resistant to chemical or enzymatic hydrolysis. As a consequence, pretreatment processes, namely bio- or physical–chemical processes to expose the lignin, must be employed. Several pre-treatment strategies have been proposed, such as steam explosion, microwave and gamma-ray irradiation, and high-energy (MeV) electron beams, among others.
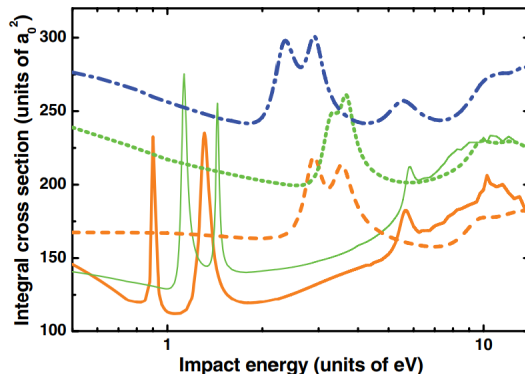

Figure 15: ICSs for elastic electron scattering by lignin components. Results for phenol are shown in orange, while the results for guaiacol and for p-coumaryl alcohol are shown in green and blue, respectively. The SE calculations are represented by the dashed lines and the SEP calculations are represented by a thick solid line [56].

Recent work from de Oliveira *et al.* [56] on the shape resonance spectra of the lignin components phenol, guaiacol and p-coumaryl alcohol in the gas phase indicated that all mentioned subunits presented three to four long-lived π^* resonances on the energy range presented (Fig. 15), suggesting that LEEs could efficiently transfer energy into the lignin matrix, eventually inducing dissociation processes. Therefore, the presence of shape resonances on the forementioned molecules might provide insight into electron-transfer processes that may be of help for biomass delignification.

To obtain the ICSs, de Oliveira *et al.* used the SMCPP method. The calculations were performed at the static-exchange (SE) and the SEP levels of approximation. The results are presented in the figure 15. Further discussion regarding the results obtained for the lignin subunits, as well as LEE scattering by cellulose and hemicellulose components can be found elsewhere [56, 57].

5.2   DNA Damage

Interaction of low energy electrons with DNA nucleobases (thymine, adenine, cytosine, and guanine), organic acids, and amino acids is of great significance for the description of the molecular mechanisms in radiation damage [58, 59]. When high-energy radiation interacts with a biological medium, it produces free radicals

and low energy electrons. This is a particularly important process in aqueous solutions as the biological damage induced by free radicals from the radiolysis of water far exceeds that by direct energy deposition to DNA [60] . Whereas the role of free radicals in the radiation damage has been well established, the role of low energy electrons is still under intense investigations. The important work of Sanche and co-workers [53, 61] has shown that damage to nucleic acids from ionizing radiation (single and double strand breaks in particular) can be generated through a mechanism involving low energy electron attachment to the nucleic acid and subsequent bond breaking due to energy transfer to a vibrational mode of the temporary anion formed in the electron-capture step. These low-energy secondary electrons are generated by electron-impact ionization caused by high-energy electrons, originally produced directly by the ionizing radiation.

A first general feature on which there is a wide agreement is that the electron capture is mainly due to the DNA and RNA bases. These molecules have extended aromatic systems; therefore there is a wide range of low-lying unoccupied π^* orbitals where an electron can be captured, giving rise to a shape resonance, in the range of energies between 0 and 15 eV, where the experiments have found signatures of electron-induced damage to nucleic acids. Given the many low-lying unoccupied orbitals in DNA bases, it is not surprising that their elastic cross sections for electron scattering exhibit many shape resonances (Figure 16).
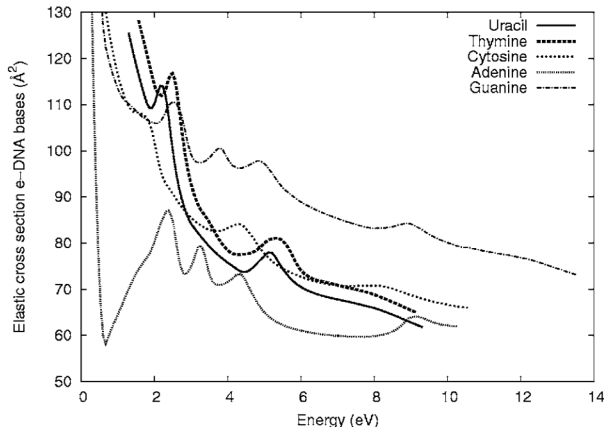

Figure 16: Partial elastic cross section for five DNA and RNA bases. The resonances are represented as the sharp peaks in all the bases considered [62].

Below about 15 eV, electrons can temporarily attach at specific energies to DNA and its fundamental subunits. In short oligonucleotides, the incoming LEE can be captured, with similar probabilities, by the phosphate group or by a base. In long duplex DNA or plasmids, electrons with energies below 15 eV are mostly captured by a base, forming a transient anion (TA) of that base. Below 4 eV, only shape resonances can locate an electron in an otherwise unfilled orbital of a base since electronic excitation is not energetically possible. Martin *et al.* [63] reported the presence of two maxima at 0.8 and 2.2 eV in plasmid DNA. These enhancements were interpreted as shape resonances, resulting from electron attachment into the otherwise empty π^* valence molecular orbitals of the DNA bases. Dissociation of the base TA can produce an abasic site or a base damage (BD) [64]. As predicted theoretically, single strand breaks (SSBs) can also occur due to

electron transfer from this π^* orbital to a low-lying $\sigma*$ orbital of the phosphate group, forming a dissociative TA at that site [65]. At higher energies up to about 15 eV, this type of process occurs via core-excited resonances, from which an electron can also transfer to the sugar-phosphate group [65, 66]. Thus, over the entire 0–15 eV range, a TA formed on a base can dissociate via DEA producing an abasic site or a BD [66]. Moreover, an electron can autodetach from a base TA, while leaving the base in a dissociative electronic excited state. The detaching electron can also transfer to another fundamental unit, where DEA can occur [65, 66].

Thus, understanding LEE-induced processes in DNA has implications, not only in the description of the physico-chemical stage of energy deposition, but also in explaining the production of DNA lesions potentially lethal to cells during the initial energy deposition process.

6   Challenges

A rich body of literature is dedicated to the fundamentals of scattering processes at electron impact energies below 100 eV. These have provided a great deal of information on collisional phenomena, cross sections, resonances and final states and products. Although the atomic and molecular physics community is still actively involved in several research endeavors, there are experimental and computational challenges that remain and potential opportunities to extend established experimental and theoretical methodologies to advance our understanding. Therefore, despite the progress achieved in both hardware and software over the last decades, there is a constant increase on the sophistication of scattering techniques and on the complexity of the systems of interest, imposing limits theoretically and experimentally, reflected in disagreements on the cross sections of targets (Figure 17).
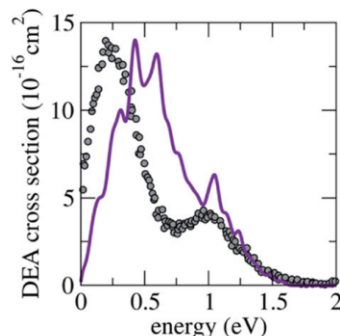
Figure 17: Calculated (purple curve) and experimental (open circle) DEA cross sections for iodoethene [67].

For scattering calculations, there are problems regarding the difficulty in describing molecular bound states. An example can be observed when we take into account the electronic correlation in LEE's interactions with molecules. Apart from the need to describe the electronic state of the target, the many-body scattering methods, like the SMC and R- matrix techniques, require additional computational costs by taking into account the appropriate boundary conditions.

There are experimental challenges regarding the accuracy of the measurements for LEE scatterring processes, such as: absolute cross sections and rates for polyatomic molecules; electronic excitations of molecules near energy thresholds; and the position, lifetime and width of the resonances for molecules.

In view of the biological relevance of the process of DEA, experimental and theoretical studies of electron interactions with aggregates become increasingly important. Therefore, besides the gas-phase state, the description of clusters and condensed-phase systems is of considerable relevance, and imposes additional challenges to be considered. An extensive discussion about theoretical challenges is found in the work of Ptasinska *et al.* (2022) [67].

7 Conclusions

Resonances play a major role on the DEA process occurring in many important applied contexts, particularly gas discharges, plasmas, biological systems, and astrophysical environments. The comprehension of the mechanisms that leads to the resonant states and the inherent difficulties in its determination provides a deeper insight into the scattering process itself.

The methods mentioned throughout this work were chosen by the wide range of articles results where the techniques were employed. As a special mention, studying the SMC and SMCPP methods provided a better understanding of the theory outlined by the methods, which plays a major role on future researches. The history of the research of LEE scattering resonances is a reflection of the technology advances throughout the decades, with better resolution and computational power, but also with new methods developed and improvements on already existing ones. The possibility of DEA of molecular targets due to resonances have several applications. We restrain our attention to the effects of resonances on the lignin molecule, which might provide insight and help biomass delignification, and on DNA bases, since DEA can cause damages on the DNA, which may lead to cellular death.

There are still limitations on providing reliable cross sections for multielectronic systems, but progress is continually obtained, with different targets studied and with state of the art equipment and methods. Previously applied only for atoms or diatomic molecules in the gas phase state, resonances are now being applied to complex multielectronic systems, allowing its use in fields such as medical, astrophysical, biofuel production and atmospheric physics.

References

[1] A. Richter. *Progress in Particle and Nuclear Physics*, **13**:1, 1985.

[2] M. Vinodkumar, C. Limbachiya, K. N. Joshipura, B. Vaishnav, and S. Gangopadhyay. *Journal of Physics: Conference Series*, **115**:012013, 2008.

[3] F. E. Harris. *Annual Review of Physical Chemistry*, **23**:415, 1972.

[4] K. N. Joshipura and N. Mason. *Atomic-Molecular Ionization by Electron Scattering: Theory and Applications.* Cambridge: Cambridge University Press, 2019.

[5] M. B. Kiataki, M. T. do N. Varella, M. H. F. Bettega, and F. Kossoski. *The Journal of Physical Chemistry A*, **124**:8660, 2020.

[6] V. I. Lend'el, V. T. Navrotskiǐ, and E. P. Sabad. *Soviet Physics Uspekhi*, **30**:220, 1987.

[7] M. Biondi, A. Herzenberg, and C. Kuyatt. *Physics Today*, **32**:44, 1979.

[8] U. Fano. *Physical Review*, **124**:1866, 1961.

[9] G. J. Schulz. *Physical Review Letter*, **10**:105, 1963.

[10] G. J. Schulz. *Reviews of Modern Physics*, **45**:378, 1973.

[11] C. Kuyatt, J. A. Simpson, and S. R. Mielczarek. *Physical Review*, **138**:A385, 1965.

[12] J. N. Bardsley and F. Mandl. *Reports on progress in physics*, **31**:471, 1968.

[13] G. J. Schulz. *Reviews of Modern Physics*, **45**:423, 1973.

[14] F. P. Bardela, A. J. da Silva, V. A. S. da Mata, M. G. P. Homem, I. Iga, R. T. Sugohara, and M. M. Fujimoto. *Journal of Physics B: Atomic, Molecular and Optical Physics*, **54**:075203, 2021.

[15] K. Takatsuka and V. McKoy. *Phys. Rev. A*, **24**:2473, 1981.

[16] K. Takatsuka and V. McKoy. *Phys. Rev. A*, **30**:1734, 1984.

[17] C. Winstead, Q. Sun, P. G. Hipes, M. A. P. Lima, and V. McKoy. *Australian journal of physics*, **45**:325, 1992.

[18] M. H. F. Bettega, L. G. Ferreira, and M. A. P. Lima. *Phys. Rev. A*, **47**:1111, 1993.

[19] R. da Costa, F. J. da Paixão, and M. Lima. *Journal of Physics B: Atomic, Molecular and Optical Physics*, **38**:4363, 2005.

[20] M. A. P. Lima, T. L. Gibson, V. McKoy, and W. M. Huo. *Phys. Rev. A*, **38**:4527, 1988.

[21] M. A. P. Lima, T. L. Gibson, K. Takatsuka, and V. McKoy. *Phys. Rev. A*, **30**:1741, 1984.

[22] E. P. Wigner and L. Eisenbud. *Phys. Rev.*, **72**:29, Jul 1947.

[23] P. G. Burke, A. Hibbert, and W. Robb. *Journal of Physics B: Atomic and Molecular Physics*, **4**:153, 2001.

[24] P. G. Burke, I. Mackey, and I. Shimamura. *Journal of Physics B: Atomic and Molecular Physics*, **10**:2497, 1977.

[25] M. Tarana, P. Wielgus, S. Roszak, and I. I. Fabrikant. *Phys. Rev. A*, **79**:052712, 2009.

[26] J. Tennyson. *Physics Reports*, **491**:29, 2010.

[27] W. Brigg. R-matrix calculations of electron-molecule collisions: flexible implementation and practice. 03 2018.

[28] A. Loupas and J. D. Gorfinkiel. *Phys. Chem. Chem. Phys.*, **19**:18252, 2017.

[29] M. J. Brunger and S. J. Buckman. *Physics Reports*, **357**:215, 2002.

[30] R. W. Ricci, M. Ditzler, and L. P. Nestor. *Journal of chemical Education*, **71**:983, 1994.

[31] S. T. Lai and C. Miller. *AIP Advances*, **10**:095324, 2020.

[32] C. Szmytkowski and P. Mozejko. *The European Physical Journal D*, **74**:90, 2020.

[33] S. Trajmar, D. F. Register, and A. Chutjian. *Physics Reports*, **97**:219, 1983.

[34] D. E. Golden, N. F. Lane, A. Temkin, and E. Gerjuoy. *Rev. Mod. Phys.*, **43**:642, 1971.

[35] M. Dampc, A. R. Milosavljević, I. Linert, B. P. Marinković, and M. Zubek. *Phys. Rev. A*, 75.

[36] M. Allan, K. R. Asmis, D. B. Popovic, M. Stepanovic, N. J. Mason, and J. A. Davies. *Journal of Physics B: Atomic, Molecular and Optical Physics*, **29**:4727, 1996.

[37] L. Vuskovic, S. Trajmar, and D. F. Register. *Journal of Physics B: Atomic and Molecular Physics*, **15**:2517, 1982.

[38] G. Balucani, N.and Capozza, F. Leonori, E. Segoloni, and P. Casavecchia. *International Reviews in Physical Chemistry*, **25**:109, 2006.

[39] A. Lun, X. J. Chen, L. J. Allen, and K. Amos. *Phys. Rev. A*, **49**:3788, 1994.

[40] W. Sun, M. A. Morrison, W. A. Isaacs, W. K. Trail, D. T. Alle, R. J. Gulley, M. J. Brennan, and S. J. Buckman. *Phys. Rev. A*, **52**:1229, 1995.

[41] P. G. Burke and H. M. Schey. *Phys. Rev.*, **126**:147, 1962.

[42] G. J. Schulz. *Phys. Rev. Lett.*, **13**:583, 1964.

[43] L. Sanche and P. D. Burrow. *Phys. Rev. Lett.*, **29**:1639, 1972.

[44] P. G. Burke. *Phys. Rev.*, **183**:245, 1969.

[45] E. T. Hudson, K. Bartschat, M. P. Scott, P. G. Burke, and V. M. Burke. *Journal of Physics B: Atomic, Molecular and Optical Physics*, **29**:5513, 1996.

[46] S. Cvejanovic, J. Comer, and F. H. Read. *Journal of Physics B: Atomic and Molecular Physics*, **7**:468, 1974.

[47] J. N. H. Brunt, G. C. King, and F. H. Read. *Journal of Physics B: Atomic and Molecular Physics*, **10**:1289, 1977.

[48] R. E. Kennerly, R. J. Van Brunt, and A. C. Gallagher. *Phys. Rev. A*, **23**:2430, 1981.

[49] J. Yoon, M. Song, J. Han, S. H. Hwang, W. Chang, B. Lee, and Y. Itikawa. *Journal of Physical and Chemical Reference Data*, **37**:913, 2008.

[50] M. A. Morrison, R. W. Crompton, B. C. Saha, and Z. Lj Petrovic. *Australian journal of physics*, **40**:239, 1987.

[51] J. N. Bardsley, A. Herzenberg, and F. Mandl. *Proceedings of the Physical Society*, **89**:305, 1966.

[52] I. Eliezer, H. S. Taylor, and J. K. Williams. *The Journal of Chemical Physics*, **47**:2165, 1967.

[53] B. Boudaïffa, P. Cloutier, D. Hunting, A. H. Huels, and L. Sanche. *Science*, **287**:1658, 2000.

[54] A. Gauf, L. R. Hargreaves, A. Jo, J. Tanner, M. A. Khakoo, T. Walls, C. Winstead, and V. McKoy. *Phys. Rev. A*, **85**:052717, 2012.

[55] C. J. Colyer, V. Vizcaino, J. P. Sullivan, M. J. Brunger, and S. J. Buckman. *New Journal of Physics*, **9**:41, 2007.

[56] E. M. de Oliveira, d'A. S. Sergio, M. H. F. Bettega, A. P. P. Natalense, M. A. P. Lima, and M. T. do N. Varella. *Phys. Rev. A*, **86**:020701, 2012.

[57] E. M. de Oliveira, R. F. da Costa, S. d'A. Sanchez, A. P. P. Natalense, M. H. F. Bettega, M. A. P. Lima, and M. T. do N. Varella. *Phys. Chem. Chem. Phys.*, **15**:1682, 2013.

[58] H. Abdoul-Carime, S. Gohlke, and E. Illenberger. *Phys. Rev. Lett.*, **92**:168103, 2004.

[59] S. Ptasińska, S. Denifl, P. Scheier, and T. D. Märk. *The Journal of Chemical Physics*, **120**:8505, 2004.

[60] T. Ito, S. C. Baker, C. D. Stickley, J. G. Peak, and M. J. Peak. *International Journal of Radiation Biology*, **63**:289, 1993.

[61] P. L. Levesque, M. Michaud, and L. Sanche. *Nuclear Instruments and Methods in Physics Research Section B: Beam Interactions with Materials and Atoms*, **208**:225, 2003.

[62] S. Tonzani and C. H. Greene. *The Journal of Chemical Physics*, **124**:054312, 2006.

[63] F. Martin, P. D. Burrow, Z. Cai, P. Cloutier, D. Hunting, and L. Sanche. *Phys. Rev. Lett.*, **93**:068101, 2004.

[64] Z. Li, Y. Zheng, P. Cloutier, L. Sanche, and J. R. Wagner. *Journal of the American Chemical Society*, **130**(17):5612, 2008.

[65] Y. Zheng, J. R. Wagner, and L. Sanche. *Phys. Rev. Lett.*, **96**.

[66] Y. Dong, Y. Gao, W. Liu, T. Gao, Y. Zheng, and L. Sanche. *The Journal of Physical Chemistry Letters*, **10**:2985, 2019.

[67] S. Ptasinska, M. T do N Varella, M. A Khakoo, D. S Slaughter, and S. Denifl. *The European Physical Journal D*, **76**:1, 2022.